Biochimica et Biophysica Acta 1847 (2015) 364–376

Contents lists available at ScienceDirect

Biochimica et Biophysica Acta

journal homepage: www.elsevier.com/locate/bbabio

How cytochrome c oxidase can pump four protons per oxygen molecule at high electrochemical gradient

Margareta R.A. Blomberg *, Per E.M. Siegbahn

Department of Organic Chemistry, Arrhenius Laboratory, Stockholm University, SE-106 91 Stockholm, Sweden

ARTICLE INFO

Article history:
Received 27 September 2014
Received in revised form 18 November 2014
Accepted 10 December 2014
Available online 18 December 2014

Keywords:
Cytochrome c oxidase
Proton pumping
Density functional theory
Energy profile
Reduction potential

ABSTRACT

Experiments have shown that the A-family cytochrome c oxidases pump four protons per oxygen molecule, also at a high electrochemical gradient. This has been considered a puzzle, since two of the reduction potentials involved, Cu(II) and Fe(III), were estimated from experiments to be too low to afford proton pumping at a high gradient. The present quantum mechanical study (using hybrid density functional theory) suggests a solution to this puzzle. First, the calculations show that the charge compensated Cu(II) potential for Cu_B is actually much higher than estimated from experiment, of the same order as the reduction potentials for the tyrosyl radical and the ferryl group, which are also involved in the catalytic cycle. The reason for the discrepancy between theory and experiment is the very large uncertainty in the experimental observations used to estimate the equilibrium potentials, mainly caused by the lack of methods for direct determination of reduced Cu_B. Second, the calculations show that a high energy metastable state, labeled $\mathbf{E}_H$, is involved during catalytic turnover. The $\mathbf{E}_H$ state mixes the low reduction potential of Fe(III) in heme a_3 with another, higher potential, here suggested to be that of the tyrosyl radical, resulting in enough exergonicity to allow proton pumping at a high gradient. In contrast, the corresponding metastable oxidized state, $\mathbf{O}_H$, is not significantly higher in energy than the resting state, **O**. Finally, to secure the involvement of the high energy $\mathbf{E}_H$ state it is suggested that only one proton is taken up via the K-channel during catalytic turnover.

1. Introduction

Cytochrome c oxidase (CcO), the terminal enzyme in the respiratory chain, is located in the inner mitochondrial or bacterial membrane. It uses electrons from cytochrome c to reduce molecular oxygen to water in an exergonic process. The electron donor, cytochrome c, is located on the P-side of the membrane (intermembrane space or periplasm), and the protons for water formation are taken from the opposite side of the membrane, the N-side (matrix or cytoplasm). Thus, the chemistry corresponds to a charge translocation across the membrane, which is referred to as an electrogenic reaction. Furthermore, the chemistry is coupled to the translocation of protons across the entire membrane, from the N-side to the P-side, referred to as proton pumping. Both the electrogenic chemistry and the proton pumping contribute to the buildup of an electrochemical gradient across the membrane, resulting in efficient conservation of the free energy. Experimental information shows that in the A-family CcOs, one proton is pumped per electron, giving the overall reaction:

$$O_2 + 8H_N^+ + 4e_P^- \rightarrow 2H_2O + 4H_P^+. \quad (1)$$

Both the electrogenic chemistry and the proton pumping correspond to moving charges against the electrochemical gradient, which means that there has to be specific mechanisms for gating the protons to move in the right direction. Many aspects of such mechanisms for proton pumping still remain to be explained. One remaining difficulty is to understand how the free energy released in reaction (1) is distributed over the catalytic cycle, so that all four reduction steps actually can be coupled to proton pumping also with a substantial electrochemical gradient present. The latter problem is a main target for the present study.

In Fig. 1 an overview of the electron and proton flow in A-family CcOs is given. The chemistry occurs in the binuclear active site, the BNC, consisting of a high-spin heme a_3 group and a mono-nuclear copper complex, Cu_B. The Cu_B complex has three histidine ligands, one of which is cross-linked to a tyrosine residue, which is considered to be redox active. The electrons are transferred from cytochrome c to the BNC via two other metal cofactors, a dinuclear copper complex, Cu_A, and a low-spin heme a. The protons are taken up from the N-side of the membrane via two proton channels, the D-channel and the K-channel. All pumped protons, and at least two of the protons for the chemistry use the D-channel, and at least one proton for the chemistry uses the K-channel. In Fig. 2 the general view of the catalytic cycle of CcO is depicted. Starting from the resting state, referred to as the oxidized state and labeled **O**, two electrons have to be taken up before molecular

* Corresponding author. Tel.: +46 8 16 26 16.
E-mail address: mb@organ.su.se (M.R.A. Blomberg).

http://dx.doi.org/10.1016/j.bbabio.2014.12.005
0005-2728/

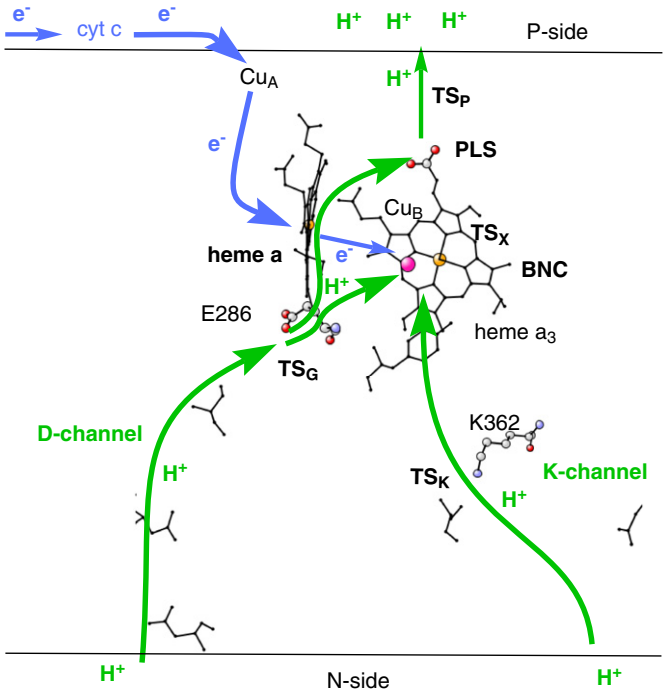

Fig. 1. Overview of electron and proton transfer in CcO (A-family).

oxygen can enter and bind to the reduced state **R**. Oxygen binds reversibly to the ferrous heme a_3, yielding the observed intermediate labeled **A**. The cleavage of the O – O bond gives intermediate $\mathbf{P}_M$ with a tyrosyl radical. After two more reduction steps the reaction is back to intermediate **O**.

With cytochrome c as the electron donor, reaction (1) becomes exergonic by 51 kcal/mol (2.2 V) [1]. With a maximum gradient of 200 mV [1], there is in principle enough energy to pump four protons per oxygen molecule also when the gradient is at its maximum, still resulting in an exergonicity of 0.6 V (13.8 kcal/mol). However, the four reduction steps, described in Fig. 2, are not equivalent, which means that the free energy is not evenly distributed over the catalytic cycle. In fact, experimental information on equilibrium reduction potentials, indicate that the two reduction steps from **O** to **R** should be only slightly exergonic already without the gradient, since the two reduction potentials involved (Cu(II) and Fe(III)) seem to be only slightly larger than that of the electron donor cytochrome c [1–4]. These two reduction steps would be endergonic with the gradient present, since both the electrogenic chemistry and the proton pumping make the reduction steps more endergonic when the gradient is present. This means that the rate limiting proton transfer barriers, and/or the O – O bond cleavage barrier would become too high for a reasonable reaction rate. Depending on which of the experimental values for the reduction potentials are considered, the rate would be on the order of hours or even days when the gradient is approaching its maximum value. Thus two sets of experimental data are seemingly incompatible, the observation that the A-family CcOs actually pump four protons with a substantial gradient present [5,6], and the observation that the reduction potentials in two of the reduction steps seem to be too low to allow high gradient proton pumping [3,4]. To solve this problem it has been suggested that there exist two different states for the oxidized intermediate **O** (and possibly also for the one electron reduced intermediate **E**), one referred to as the activated state, which appears immediately after the reaction with molecular oxygen, and with a limited life time, and another one referred to as the resting state, which is lower in energy than the activated state, and which is formed from the activated state if the flow of electrons is stopped. The activated state, labeled $\mathbf{O}_H$, has thus been suggested to have a higher reduction potential than the resting state, **O**, and it has also been suggested that, in contrast to state $\mathbf{O}_H$, the **O** state does not pump protons [7,8]. So far, however, it has not been possible to establish any differences in reduction potentials or spectroscopic properties between the two states [3].

To understand the mechanisms for proton pumping and energy conservation in CcO it would be useful to know more details about the intermediates in the catalytic cycle. In this context quantum chemistry can contribute by calculating relative energies, electronic and geometric structures of possible intermediates. In particular, the experimental value for the reduction potential of Cu(II) in CcO is quite uncertain, since there is no direct way to determine this value. Therefore, quantum chemistry may be used to improve the information about the problematic reduction potentials mentioned above. However, calculations on this type of complicated reactions are very challenging, and it is not possible to rely only on the calculations to obtain accurate information. The results from quantum chemical calculations need to be combined with some of the experimental information available. The main difficulty is that *absolute* reduction potentials cannot be determined accurately from calculations, and therefore experimental reduction potentials are used to obtain the overall exergonicity of the O_2 reduction in CcO, while hybrid density functional theory (B3LYP) is used to obtain relative energies of the reduction steps. This procedure has been used in several previous quantum chemical studies on CcO and other systems [9–14]. In particular, the same approach was successfully used to solve the mechanism for water oxidation in PSII [15]. Further details about the procedures used to connect the results from the calculations with experimental information are given in Appendix A.

In the present study, the results from quantum chemical calculations are used to obtain a detailed picture of O_2 reduction in the A-family CcOs. One of the main conclusions is that the charge compensated reduction potential for Cu(II) is significantly larger than concluded from the indirect equilibrium measurements, and it is suggested that the new result is compatible with the uncertainty of the experimental observations. Furthermore, for the **O** and **E** intermediates, possible structures are suggested for both the so called activated, metastable states involved in catalytic turnover, and the resting states involved in the equilibrium experiments. The directly calculated free energy profile for the catalytic cycle corresponds to the situation without any gradient present. The energetic effects on the energy profile from a gradient corresponding to about 85% of the maximum value (i.e. 170 mV) is added to the calculated relative energies to estimate the energetics with a significant gradient present. The results show that the reduction mechanism suggested, based on new structures for all intermediates in the entire catalytic cycle, gives rise to a free energy profile which is compatible with proton pumping in all four reduction steps also when a substantial electrochemical gradient is present. Thus the results presented suggest a solution to the puzzle discussed above for the seemingly incompatible experimental information.

2. Results and discussion

A model of the BNC is built on the basis of a recent crystal structure [16], see Fig. 3 and Appendix A. As further discussed in the appendix the model is chosen to represent the intrinsic reaction energies for the O_2 reduction reaction in cytochrome oxidase. It should be stressed that long-range effects do not significantly modify the relative energies of this reaction, which are the only values that matter here. Using this model all steps in the catalytic cycle of oxygen reduction were studied, including an explicit description of both electron and proton transfer states in each reduction step. Several structures and states of each intermediate were characterized, and in Fig. 4 the structures suggested to be part of the catalytic cycle during turnover are summarized. The most interesting aspect of this reaction scheme is that it yields an energy profile compatible with proton pumping in all four reduction steps, also with a substantial gradient, indicating, among other things, that the Cu(II) potential is significantly higher than previously estimated

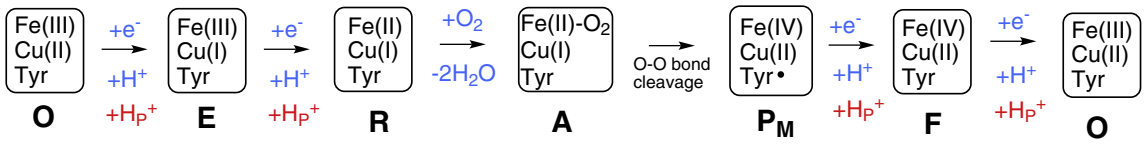

Fig. 2. General view of the catalytic cycle of CcO, starting from the oxidized state **O**. The notation H_P^+ corresponds to pumped protons.

on the basis of experiment. Other interesting observations for the reaction mechanism described in Fig. 4 are that the tyrosyl radical appears in several, rather unexpected, steps, and that the electronic structure obtained when an electron is added, changes when the corresponding proton enters the BNC.

The results are discussed in three subsections below. In the first subsection the details of the reaction scheme are presented, together with the energetics of the catalytic cycle without gradient. In the second subsection reduction potentials for the different steps are discussed, and possible differences between activated and resting states of the **O** and **E** intermediates are presented. The connection between the calculated results and the experiments performed to determine the equilibrium reduction potentials is also discussed. In the third subsection the effects of the gradient on the energy profile are discussed, and the possibility for proton pumping at high gradient is evaluated.

The model of the BNC used in the calculations, the quantum chemical methods, and the procedure used to connect the calculated relative energies to experimental data are described in Appendix A at the end. Optimized structures for all intermediates discussed below are shown in Supplementary data.

2.1. Reaction mechanism of O_2 reduction

On the basis of the calculations, a reaction mechanism for O_2 reduction during catalytic turnover in the A-family CcOs is suggested, as shown in Fig. 4. Chemical aspects of this mechanism are discussed below, while some more technical aspects concerning the different intermediates are discussed in Section A.1 in Appendix A. A free energy profile for one catalytic cycle is constructed using a combination of computational and experimental data, see Fig. 5. A few comments need to be made about this energy profile. First, as mentioned above, the overall energy is adjusted to fit the experimental value of 51 kcal/mol, which means that every second energy level, corresponding to the four reduction steps is fixed from the calculations. The details of this procedure is described in Section A.3 in Appendix A. To simplify the picture in Fig. 5, the intermediates involving the uptake of the protons to be pumped are not included, and also the barriers connected with the motion of the pumped protons are excluded. Since the energy profile corresponds to the situation without gradient, there is no cost for the proton pumping, and the thermodynamics is therefore not affected. However, there are significant barriers connected with transfer of the pumped protons, which means that the *rate limiting barriers*, present in each reduction steps, are missing in this energy profile. Furthermore, the barriers for electron and proton transfer to the BNC are assumed not to be rate limiting for the reduction process, and they are therefore just indicated (and not calculated). The subindex on the protons in the figure, D or K, indicates which of the two proton channels is suggested to be used in each particular step (compare Fig. 1). No proton transfer barriers are calculated using the present model, all estimates are based on experimental information.

The mechanism of the catalytic reaction in the BNC is most easily described by starting with the reduced state **R** and the binding of molecular oxygen. In **R** the ferrous iron is in a high-spin state, copper is reduced, and the two water molecules just formed are weakly coordinated to the metals. A small cost is involved in removing the waters to make space for the oxygen molecule. The energy level of the high spin Fe(II) state is shifted to make the binding of the O_2 molecule agree with experiments that indicate that this process is, at most, only weakly exergonic [17]. In the next step, the O – O bond is cleaved forming intermediate $\mathbf{P}_M$, in which all four electrons have been transferred from the BNC to oxygen. This step is calculated to be exergonic by 3.2 kcal/mol, and the barrier of 12.4 kcal/mol for the O – O bond cleavage shown in Fig. 5 is taken from experiment [18]. (The calculated barrier using the present model is somewhat higher, 17.1 kcal/mol). In $\mathbf{P}_M$ the BNC is thus in its most oxidized state with Fe(IV), Cu(II) and a tyrosyl radical. There is not much choice in geometrical or electronic structure for this state. The ferryl iron is low-spin, ferromagnetically coupled to the oxo ion. The rest of the catalytic cycle consists of the four reduction steps, each composed of an electron and a proton transfer to the active site, and the pumping of one proton across the entire membrane. The latter part of the reaction is not included in the discussion in this section.

The first reduction step after the O – O bond cleavage, including uptake of both the electron and the proton, leads to formation of intermediate **F**, and it is found to be exergonic by 18.6 kcal/mol, see Fig. 5. When only the electron is added, it goes to the tyrosyl radical, giving state $\mathbf{P}_R$. The present computational approach makes this electron transfer step only slightly exergonic, and the large exergonicity is obtained first when the proton is added. It is found to be significantly more favorable to put the proton on the OH-group in the BNC than on the tyrosinate, thus giving a water molecule in the BNC. Furthermore, with a water molecule coordinated to copper, it is more favorable for the electron to move from tyrosinate to copper, resulting in Cu(I) and a tyrosyl radical ($TyrO^\bullet$ – Cu(I)-OH_2 plus Fe(IV)═O) for the **F** intermediate, as shown in Fig. 4.

The next reduction step is initiated by electron transfer to iron forming a high-spin ferric hydroxyl group. To make this electron transfer possible, it is necessary to start with a water molecule in the BNC, such that a proton can be internally transferred to the iron coordinated oxygen during the electron transfer. This internal proton transfer leaves a hydroxyl group on copper, which in turn triggers an internal electron transfer from copper to the tyrosyl radical, giving the structure for $\mathbf{F}_R$ as shown in Fig. 4. This rather complicated step of electron transfer to the active site is slightly endergonic with the computational approach used. This result should be in accordance with the experimental observation that a positive charge in the K-channel (protonated lysine) is needed to make electron transfer to the BNC occur [19], i.e. to make it exergonic. Since the stabilizing effect of this positively charged lysine on the electron in the active site is not included in the present model, it is reasonable that this electron transfer step is slightly endergonic. Similar to the previous reduction step, when the corresponding proton enters the BNC to complete the reduction step, the hydroxyl group on copper is transformed into a water molecule. This triggers electron transfer from the tyrosinate to copper, giving Cu(I) and a tyrosyl radical ($TyrO^\bullet$ – Cu(I)-OH_2 plus Fe(III)OH) in the $\mathbf{O}_H$ intermediate. It is suggested that this structure for the intermediate is involved in the catalytic cycle during turnover, which means that it should correspond to the so called activated state, and therefore the label $\mathbf{O}_H$ is used. A closely related structure is obtained by moving the hydrogen bonding proton from the copper water ligand to the iron hydroxyl ligand (see Fig. S2), resulting in a water molecule coordinating to iron (Fe(III)-OH_2). The barrier for such proton motion should be low, and since the structure with a water ligand on iron is somewhat higher in energy than the one with a hydroxyl ligand in the present model, the Fe(III)-OH_2 type of structure is not further discussed. A distinctly different structure for the oxidized intermediate is obtained if the tyrosinate is protonated instead of the OH-group in the BNC, but in the calculations this tyrosine

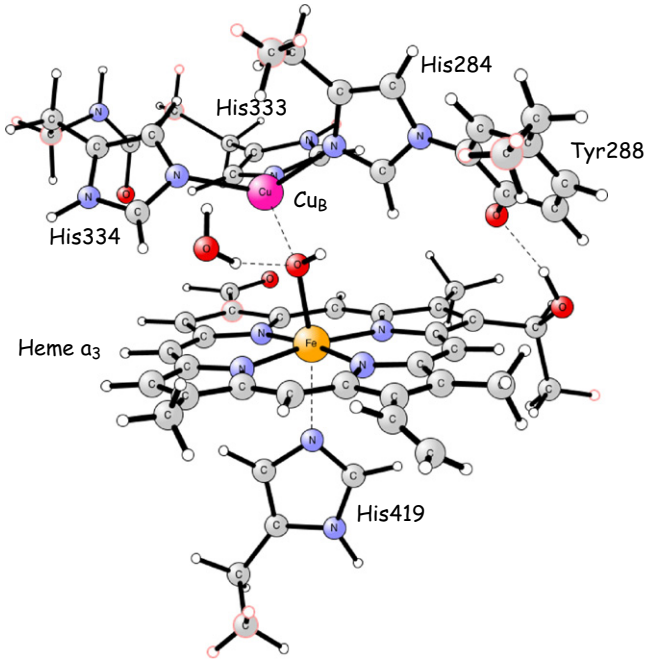

Fig. 3. Model of the BNC, built on the X-ray structure of the oxidized CcO [16] (PDB: 2GSM). The atoms with pink circles are fixed to the X-ray coordinates in the geometry optimizations.

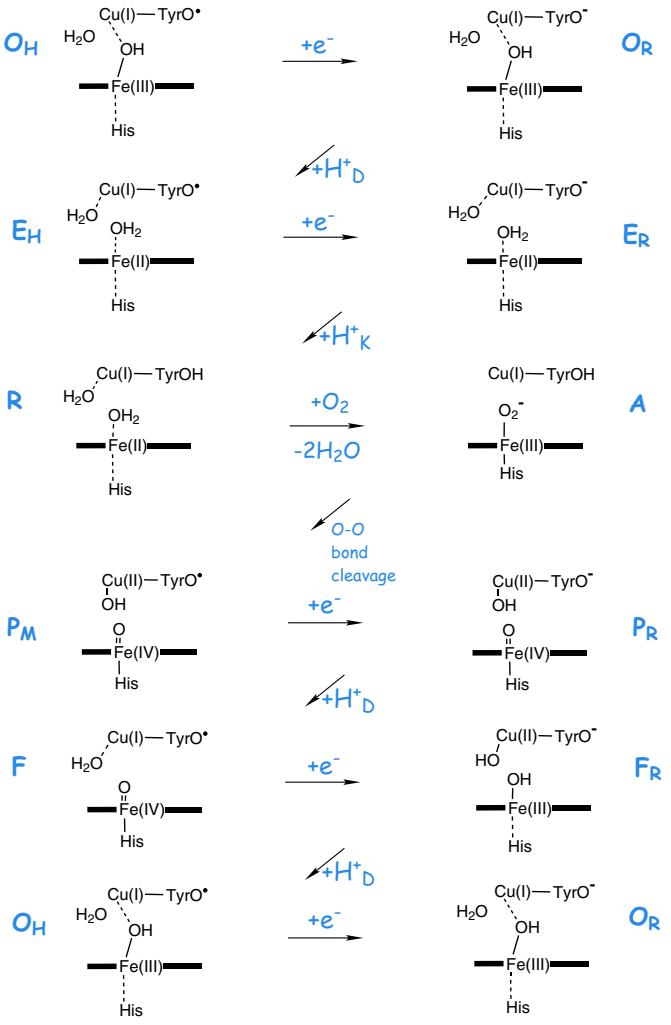

Fig. 4. Suggested reaction scheme for the catalytic cycle of CcO during turnover. The notation TyrO• represents a tyrosyl radical.

state (TyrOH–Cu(II)OH) is a few kcal/mol higher in energy than the one with a tyrosyl radical. Possible alternative states of intermediate **O** will be further discussed in Section 2.2 below. The entire reduction step as depicted in Fig. 4 is found to be exergonic by 13.1 kcal/mol. The two reduction steps just described are often referred to as the oxidative part of the catalytic cycle, while the next two steps are referred to as the reductive part.

The first step in the reductive part of the catalytic cycle, is electron transfer to the tyrosyl radical in the $\mathbf{O}_H$ state. This step is slightly exergonic, just as for the $\mathbf{P}_M$ to $\mathbf{P}_R$ transition. With this structure for the $\mathbf{O}_R$ state, see Fig. 4, there are two possibilities for the incoming proton. It can either go to the tyrosinate and form tyrosine, which actually gives the lowest energy in this case. However, this low energy state must be considered as a trap, which will be further discussed below in Section 2.2. Instead, the second alternative, with the proton going to the hydroxyl group on iron is here considered to be the one involved in the catalytic turnover, and therefore the one depicted in Fig. 4 with the label $\mathbf{E}_H$. Now, similar to the copper case above, when the hydroxyl group on Fe(III) is transformed into a water molecule, it is found to be more favorable for the electron to move from tyrosinate to iron, to form high-spin Fe(II)-OH_2 and a tyrosyl radical, which is the way the $\mathbf{E}_H$ intermediate is depicted in Fig. 4. The electronic structure of the $\mathbf{E}_H$ state is further discussed in Section 2.2 below. The entire reduction step is exergonic by 8.1 kcal/mol, which includes the lowering of the Fe(II) state as mentioned above in connection with formation of intermediate **A**. An important aspect of this suggested structure for the $\mathbf{E}_H$ state is that it implies that the proton uptake in this reduction step must occur via the D-channel during catalytic turnover, since if the proton comes via the K-channel the tyrosine trap cannot be avoided. It is therefore assumed that the barrier in the K-channel, at least at this stage of the reaction, is higher than the barrier in the D-channel. It is also required that any barrier for proton transfer from the BNC to the tyrosine is too high for the proton to be transferred this way within the time-span of this reduction step. Preliminary calculations on a larger model indicate high enough barriers to avoid such proton transfer. The assumption about the proton uptake via the D-channel in this reduction step is in accordance with the observation that this reduction step actually does occur in mutants missing the essential lysine in the K-channel [20].

In the final reduction step, both the electron and the proton go to the tyrosyl radical, and the reduced state **R** is reformed. As indicated in Fig. 5, it is suggested that this proton is taken up via the K-channel, which is natural since the K-channel ends at the tyrosine residue. It is also suggested that at this point of the reaction, the barrier for moving a proton via the D-channel is quite high. The difference between this reduction step and the three previous ones is that in this case there is no site inside the BNC itself with a high affinity for a proton. The entire reduction step is found to be exergonic by 7.0 kcal/mol, but the electron transfer step is endergonic by a few kcal/mol, which might be surprising since it could be expected to be quite similar to two of the previous reduction steps where the electron transfer occurs to the tyrosyl radical slightly exergonically. The explanation for the lower calculated electron affinity in this step is that a $TyrO^-$–Fe(III) electronic structure is actually already slightly mixing with the main $TyrO^•$–Fe(II) structure in the reactant $\mathbf{E}_H$ state, which will be further discussed in Section 2.2 below. Thus, it is suggested that this electron transfer is endergonic, and that the proton transfer in the K-channel must occur more or less concerted with the electron transfer. This would be in agreement with the experimental observation on K-channel mutants, that the final reduction cannot occur without the lysine in the K-channel [20].

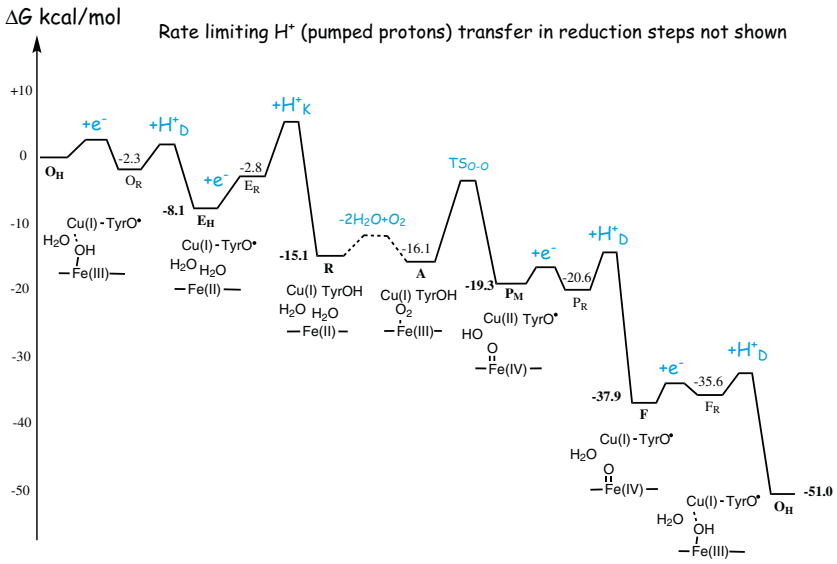

Fig. 5. Free energy profile for the catalytic cycle of CcO without gradient, based on calculated thermodynamics. The barriers for electron and proton transfer to the BNC are indicated. The subscript on the protons (D or K) indicates which channel is suggested to be used for a particular reduction step.

A few comments should be made about the reaction mechanism presented and discussed above. First, the appearance of the tyrosyl radical in several reduction steps is different from previous suggestions. This result may not be of energetic importance, since if two positions for the electron, e.g. the copper ion and the tyrosine ring, have similar energies, the electron may be in one position or the other, or even delocalized over the two parts with the same energy. However, it seems quite reasonable that the reduction potential of copper increases when a proton is added, forming water from the previous hydroxyl ligand on copper, and that the electron therefore moves from the tyrosinate to the copper ion, e.g. in the $\mathbf{P}_R$ to **F** step. As will be discussed in the next section, there are also other factors that affect the copper potential in certain intermediates. Furthermore, the reaction scheme in Fig. 4 implies that, considering the products of the full reduction step with both electron and proton transfer, the reduction of the different parts of the active site does not occur in the order generally assumed, shown in Fig. 2. On the other hand, if the states labeled $\mathbf{X}_R$, i.e. the reduced states before the proton has arrived (right column in Fig. 4), are compared to each other, it is found that in this series the reductions actually occur in the expected order. Starting with state $\mathbf{P}_R$, where the electron has just annihilated the tyrosyl radical to give a tyrosinate, the next reduction occurs at iron, going from Fe(IV) to Fe(III) to give $\mathbf{F}_R$. The next electron gives Cu(I) in $\mathbf{O}_R$ and finally Fe(II) is formed in $\mathbf{E}_R$. The possibility to observe the $\mathbf{X}_R$ states depends on the barriers for the following proton transfer steps, which might also involve the pumped protons. A crucial component of the mechanism suggested in Fig. 4 is that only a single proton, the second proton in the reductive part of the cycle, is taken up via the K-channel, since as mentioned above, proton uptake via this channel for the first step in the reductive part, would lead to an energy trap. This conclusion is in agreement with the experimental observations that at least one of the protons is taken up via the K-channel in the reductive part of the catalytic cycle, but it rules out interpretations of experimental data claiming that two protons are transferred via the K-channel during catalytic turnover.

Perhaps the most striking result presented in this section is the energetics of the catalytic cycle. As shown in the energy profile in Fig. 5 the two reduction steps in the reductive part of the cycle, **O** to **E** and **E** to **R**, are exergonic by as much as 7–8 kcal/mol. This is substantially more than the very small value (less than one kcal/mol) obtained from the experimental equilibrium reduction potentials [3], but still less than the 13–19 kcal/mol obtained for the two reduction steps in the oxidative part. This result indicates that the reduction potentials for the intermediates involved in the reaction mechanism described above are substantially larger than those suggested by the equilibrium measurements. This in turn raises two questions. First, if the states involved in the reaction mechanism described above correspond to the suggested $\mathbf{O}_H$ and $\mathbf{E}_H$ states, what are the structures of the corresponding resting states, **O** and **E**, and what are the reduction potentials of the different states? Second, is the energy profile presented in Fig. 5 compatible with the high level of proton pumping at a high gradient as obtained in certain experiments? These two questions are discussed in the two following subsections.

2.2. Reduction potentials and different structures of the O and the E intermediates

As mentioned in the introduction, experimental information on the equilibrium reduction potentials in the reductive part of the catalytic cycle (**O** to **E** and **E** to **R**) indicates that these potentials are too low to afford proton pumping. Still, proton pumping is observed for these reduction steps, and therefore it has been speculated that the intermediates for these reduction steps also exist as metastable, so called activated states, with higher reduction potentials. As will be further discussed in the next section, the calculated energy profile in Fig. 5 gives a different picture with regard to proton pumping than that expected from the experimental reduction potentials. Therefore, the results from the previous section are discussed below in terms of corresponding reduction potentials for the intermediates involved. Comparisons to experimental data show that the calculated reduction potentials agree quite well with experimentally determined reduction potentials, except for the case of Cu(II), which is the most uncertain of the experimental results. It is suggested below that the calculated value for Cu(II), which is significantly higher than the values deduced from experimental observations, may be compatible with the uncertainties in the experimental measurements. Possible alternative states for the intermediates are also presented and discussed.

The reaction scheme in Fig. 4 shows that each reduction step, including both the electron uptake and the proton uptake, corresponds to the formation of a new O – H bond. Thus the strength of the O – H bond gives a measure of the relative reduction potential involved in each reduction step. These reduction potentials involve the chemistry taking place in the active site of CcO, in contrast to reduction potentials determined for single ions in solution and for many other protein cofactors. As further described in Appendix A, the procedure used here to adjust the

calculated energetics to the experimental overall exergonicity for one catalytic cycle, corresponds to setting a value for the combined cost of an electron from cytochrome c and a proton from bulk, which at the computational level used in the present study gives a value of 67.8 kcal/mol. The difference between the calculated O – H bond strength and the cost of the electron and the proton (67.8 kcal/mol) gives the exergonicity of the reduction step, as shown in Fig. 5. From this energy difference, and the reference value of 0.25 V for the electron donor cytochrome c, the calculated O – H bonds can be transformed into reduction potentials (or midpoint potentials), listed in Table 1 in the order they appear in the scheme in Fig. 4. All reduction potentials mentioned here include both electron transfer and proton uptake, denoted charge compensated reduction potentials. For comparison, the BNC model is separated into two complexes, a heme complex and a copper complex (including the cross-linked tyrosine), see Fig. S1, and the corresponding O – H bond strengths are calculated using these two models. The resulting O – H bond strengths can be transformed to reduction potentials using the same reference values as for the BNC model, and the values obtained are listed in the last column in Table 1. The values calculated in this way for the separated complexes should reflect the inherent reduction potentials for the different cofactors in the chemical form relevant for the CcO active site. The corresponding values for the combined BNC model shows how these inherent reduction potentials are modulated by the immediate surrounding in the active site, i.e. by the interaction between the two parts of the BNC model, such as hydrogen bonding and charge transfer. Clearly, the reduction potentials can be further modulated by the surrounding protein not included in the present BNC model, but these effects are expected to be small for these charge compensated reduction potentials. The relative reduction potentials reported should be considered as reference values for the CcO active site, expected to give a qualitatively correct picture, but they are not claimed to be of high quantitative accuracy for the working enzyme. For comparison experimentally reported reduction potentials for the different reduction steps are summarized in Table 2.

In some steps in the catalytic cycle there is a choice of which reduction process should occur. Different reduction processes in a particular step will lead to different energetics for the O – H bonds and thus to different midpoint potentials, due to differences in hydrogen bonding and state mixing. The values given in parenthesis in Table 1 give these ranges of possible results. These choices are essentially connected to in which step the tyrosine is reformed, i.e. at what stage the tyrosine proton is allowed to enter and consolidate the reduction of tyrosine. Tyrosine formation can occur already in the **F** intermediate, but this structure (TyrOH – Cu(II)OH) is much less stable than the TyrO$^{\bullet}$–Cu(I)-OH_2 structure suggested in Fig. 4 for the **F** intermediate, and it should not be of further interest. Also for the oxidized state (labeled **O** or $\mathbf{O}_H$) the calculations give a lower energy for the tyrosyl radical structure (TyrO$^{\bullet}$–Cu(I)-OH_2) than for the tyrosine structure (TyrOH–Cu(II)OH), but in this case the calculated energy difference between the two structures is smaller. In the one electron reduced intermediate (labeled **E** or $\mathbf{E}_H$), on the other hand, the tyrosine structure (TyrOH–Fe(III)OH) turns out to be significantly more stable than the tyrosyl radical structure (TyrO$^{\bullet}$–Fe(II)-OH_2), suggested to be involved in the reaction scheme above. These results suggest that the most plausible alternative structures for the two intermediates **O** and **E**, apart from the ones given in Fig. 4, are the ones with a tyrosine rather than a tyrosyl radical. Using the calculated energetics for these different states, an energy profile for only the reductive part of the catalytic cycle is constructed in Fig. 6. From this energy profile several interesting conclusions can be made.

For the oxidized intermediate (labeled **O** or $\mathbf{O}_H$) the calculations give a somewhat higher energy for the TyrOH–Cu(II)OH state than for the TyrO$^{\bullet}$–Cu(I)-OH_2 state. An important difference between these two states is that the electron affinity (electron uptake without charge compensation) is very low for the TyrOH–Cu(II)OH state, while it is significantly larger for the TyrO$^{\bullet}$–Cu(I)-OH_2 state. In the TyrO$^{\bullet}$–Cu(I)-OH_2 state, the added electron goes to the tyrosyl radical, which has a high electron affinity. In the TyrOH–Cu(II)OH state the electron goes to Cu(II)OH, which has a low electron affinity when there is no "extra" proton available in the BNC that can lead to formation of a water ligand on copper. It is suggested that reduction of the **O** state will have to start with a proton transfer from the tyrosine to the BNC itself, which is denoted as H^{+}_{B} in Fig. 6, forming the $\mathbf{O}_H$ state. Based on these differences in properties it is suggested that the experimentally observed resting state, labeled **O** has the TyrOH–Cu(II)OH structure, as depicted in Fig. 6, and the activated $\mathbf{O}_H$ state has the TyrO$^{\bullet}$–Cu(I)-OH_2 structure, and is involved in enzyme turnover as suggested in the reaction scheme above. Clearly, if a resting state different than the one involved in the catalytic cycle at all appears, which is indicated by experiment, it should be lower in energy than the activated state, which is in contrast to the calculations. However, the calculated energies for the two states are close enough to make it possible that the order is reversed in the actual enzyme under equilibrium conditions. Most importantly, the calculations show that it is highly unlikely that the **O** state is much lower in energy than the activated $\mathbf{O}_H$ state. This result is in contrast to the previous experimental suggestion that state **O** should be significantly lower in energy than the activated state [7,8], as indicated in Fig. 6 ($\mathbf{O}_{exp}$ in red). It is also quite unlikely that there is any other structure of the **O** intermediate with lower energy, at least not with the same number of protons as in the structures considered here. It should be noted that a high energy $\mathbf{O}_H$ state obtained by moving the water molecule to a less optimal position within the active site, as suggested on the basis of quantum chemical calculations [21], is highly unlikely to be involved during turnover. The main reason is that moving a water molecule within the active site is not expected to give a high enough barrier to prevent relaxation into the structure with the lower energy during catalytic turnover.

The present results for the **O** and $\mathbf{O}_H$ states mean that from a thermodynamic point of view it does not make a difference which one is formed. For the catalytic turnover the barrier between the states is not important, since no energy is lost by forming the **O** state, and since reduction of the **O** state has to occur via the $\mathbf{O}_H$ state. However, to explain certain experimental observations [7,8] the barrier has to be high enough to give the $\mathbf{O}_H$ state a long enough life-time. At the same time the barrier must not be too high, to agree with other experimental observations [3]. In fact, the latter experimental data, indicating great similarities between the **O** and the $\mathbf{O}_H$ states [3], suggests that this barrier is of the same order as the rate limiting proton transfer barriers not shown

Table 1
Calculated reduction potentials (in V) using the O – H bond strengths, 67.8 kcal/mol as the cost for an electron and a proton, and 0.25 V for the electron donor cytochrome c as reference. Results are shown both for the BNC model, and for two models obtained by separating the heme and the copper complexes (see Fig. S1).

Transition in BNC	Reduction process	BNC model[a]	Separate heme or Cu-TyrOH model
$\mathbf{O}_H \rightarrow \mathbf{E}_H$	Fe(III)OH + H→ Fe(II)-OH_2[b]	0.60 (0.37–0.60)	0.48
$\mathbf{E}_H \rightarrow \mathbf{R}$	TyrO$^{\bullet}$ + H→ TyrOH	0.55 (0.55–0.77)	0.86
$\mathbf{P}_M \rightarrow \mathbf{F}$	Cu(II)OH + H→ Cu(I)-OH_2	1.06 (0.95–1.06)	0.64
$\mathbf{F} \rightarrow \mathbf{O}_H$	Fe(IV)=O + H→ Fe(III)OH	0.82	0.72

[a] The main values given for the BNC model are the ones corresponding to the mechanism discussed in the previous section. The values in parenthesis give the range of values obtained for each particular reduction occurring in any possible step of the catalytic cycle (see further in the text).
[b] All values involving Fe(II) include a correction of 7.6 kcal/mol as described in Section A.1 in Appendix A.

Table 2
Experimentally reported reduction potentials for the four reduction steps.

Transition in BNC	Reduction process	
O→ E	Cu(II)→ Cu(I)	0.28–0.35[a]
E→ R	Fe(III)→ Fe(II)	0.29–0.35[a]
P_M→ F	Tyr•→ Tyr	0.82–1.20[b]
F→ O	Fe(IV)→ Fe(III)	0.76–1.05[b]

[a] See ref. [2,3].
[b] See ref. [2,4].

in the energy profile in Fig. 6. Indeed, it is quite likely that the rather complicated proton motion between the two states, implied above, leads to a fairly high barrier, that very well might be of the same order as the rate limiting barriers for the pump protons.

Finally, from experiment it is known that the resting oxidized state is EPR silent, which has been suggested to be due to a strong exchange coupling between high-spin Fe(III) and the Cu(II) in the BNC [3,22]. The present calculations give essentially no energy difference between ferro- and antiferromagnetic coupling between the two metal ions, which indicates that the resting **O** state rather may have a low-spin iron. Upon reduction, iron would change to high-spin in the $\mathbf{O}_R$ state, which is formed via the high-spin $\mathbf{O}_H$ state as described above.

Similar to the oxidized intermediate, the one electron reduced intermediate with tyrosine, TyrOH–Fe(III)OH, shown in Fig. 6, is suggested to correspond to the **E** state, while the metastable, activated $\mathbf{E}_H$ state involved in the reaction mechanism shown in Fig. 4, is $TyrO^{\bullet}$–Fe(II)-OH_2. In contrast to the oxidized intermediate, for the one electron reduced intermediate, the **E** state is significantly lower in energy than the $\mathbf{E}_H$ state, indicating that the $\mathbf{E}_H$ state has a higher charge compensated reduction potential than the **E** state. It was argued above, that the low lying **E** state must be avoided during catalytic turnover. One reason for this is that it is too stable, leaving very little energy for the last reduction step. Another reason is the very low electron affinity (electron uptake without charge compensation) in the BNC, again due to the lower number of protons in the actual BNC (as discussed above in connection with the **O** state) resulting in a too high barrier for the next reduction step. Compared to the $\mathbf{E}_H$ state, the rate limiting barriers will be higher by the energy difference between the **E** and the $\mathbf{E}_H$ states, since, to make it possible for the electron to enter, the proton has to be transferred from tyrosine to the actual BNC, forming the $\mathbf{E}_H$ state, similar to what was described above for the oxidized intermediate.

To summarize, the calculations give plausible structures for two alternative states for the oxidized and the one electron reduced intermediates, where the resting state has a reduced and protonated tyrosine, and the metastable, activated state has a tyrosyl radical. An important difference to the suggestions based on experiment, though, is that for the oxidized intermediate the $\mathbf{O}_H$ state does not have much higher energy than the **O** state. Instead it is only the **E** state that has a very low energy, significantly lower than the metastable $\mathbf{E}_H$ state. To explore this difference, the energy profile for the reductive part of the catalytic cycle is simplified, showing only the resting states, expected to appear in equilibrium experiments, see Fig. 7. In this figure, each reduction step is shown as one step with a combined barrier for the electron and proton transfer. The heights of the barriers are only sketched, since these profiles will mainly be related to equilibrium measurements, which are assumed to be performed during long enough time to surmount all barriers that might be involved. The black profile in Fig. 7 is based on the calculated energy profiles in Fig. 6, focusing on the resting states **O** and **E**, which both have a protonated tyrosine. As discussed above, there is an uncertainty of a few kcal/mol for the position of the **O** state, and similarly for the **E** state. Regardless of these uncertainties, the calculated energy profile gives a very clear picture, with the **E** state significantly lower than the **O** state, and with the **R** state rather close in energy to the **E** state. The red profile in Fig. 7 is deduced from the experimental measurements, interpreted to give reduction potentials only slightly larger than that of the electron donor cytochrome c [3], which suggests that both reduction steps are exergonic by less than 1 kcal/mol. In this figure the **O** states are placed at the same energy level for the theoretical and the experimental profiles. Comparing the **O** to **E** transition between these two profiles, shows that the main difference is that the calculations give a large reduction potential for Cu(II) (on the order of 1 V, including both electron and proton uptake), while based on experiment a very low value (0.28 V) is suggested. On the other hand, for the reduction potential of Fe(III) the calculations give a similar picture as experiment, since in both cases the **E** to **R** transition has a low exergonicity, indicating a

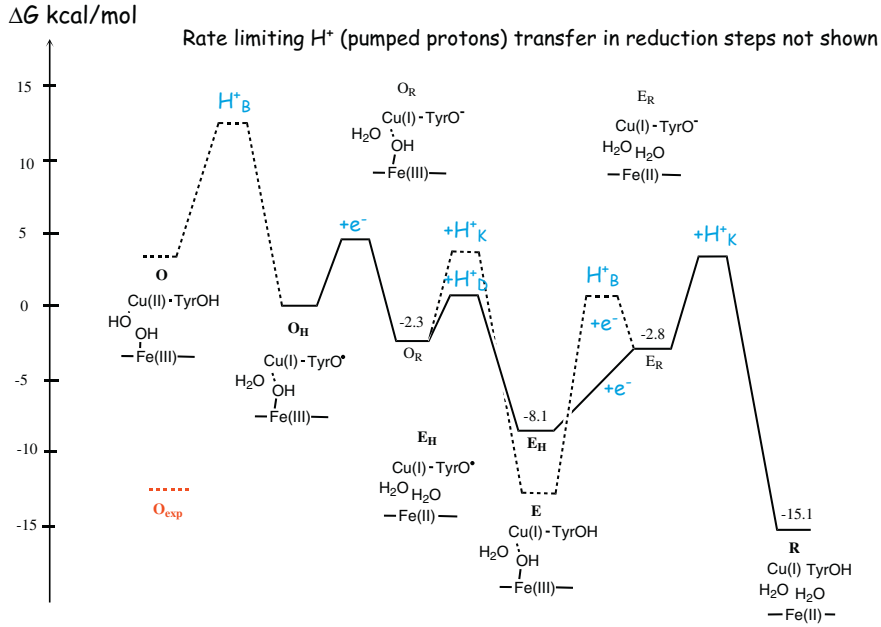

Fig. 6. Free energy profile for the reductive part of the catalytic cycle of CcO, based on calculated relative energies for different structures of the oxidized (labeled **O** or $\mathbf{O}_H$) and the one electron reduced (labeled **E** or $\mathbf{E}_H$) intermediates. The red line marked $\mathbf{O}_{exp}$ is meant to indicate the position of the resting oxidized state relative to the metastable $\mathbf{O}_H$, as suggested on the basis of experiment [7,8].

reduction potential for Fe(III) only slightly larger than for the donor cytochrome c.

Thus the main difference between the theoretical and the experimental results is that theory suggests a much higher reduction potential for copper. This raises the question if the results of the equilibrium measurements may be interpreted in a different way, in particular since the experimentally deduced reduction potential for Cu(II) is quite uncertain. In the experiment, anaerobically oxidized CcO was reduced with two equivalents of ferrocytochrome c. After equilibrium had been reached the optical spectrum was analyzed to determine the amount of different states present [3]. The results showed that there was a mixture of states, and that there was still reduced cytochrome c present (as well as reduced Cu_A and heme a). Clearly, if the **R** state was significantly lower than both the other states, only this state with all cofactors reduced, plus oxidized cytochrome c would be observed. Therefore, the experimental result shows that at least the second reduction step is not significantly exergonic. Based on the calculated black profile in Fig. 7, the expected outcome of this type of equilibrium measurement can be proposed. The **E** and **R** states have similar energy, and therefore, the product after equilibrium is a mixture of these two states. Since state **E** is only one electron reduced there is still reduced cytochrome c present at equilibrium, in agreement with the experimental observation. Furthermore, since Cu_B is reduced in both **E** and **R**, all Cu_B should be reduced, and since heme a_3 is reduced in **R** but not in **E**, heme a_3 is only partially reduced. Thus, the calculated black energy profile in Fig. 7 would indeed give rise to a distribution of the electrons over the different cofactors, which may be compatible with the experimental observations, depending on the exact proportions of the experimental distribution, and on the uncertainty in the experimental procedure to determine these proportions. Clearly, the estimated amount of reduced Cu_B in the experiment is quite uncertain, since it cannot be measured directly, but depends on the sum of estimated amounts of three other reduced cofactors, including Cu_A, which in itself is quite uncertain. Counting backwards, the reduction potentials given in the paper [3], would correspond to an estimated amount of 88% reduced Cu_B in the experiment, not very far from the 100% deduced from the calculated energy profile. In fact, due to the exponential form of the Boltzmann distribution, which determines the relation between the amount of reduced cofactor and the corresponding reduction potential, rather small uncertainties in the observed amounts of reduced cofactors lead to very large uncertainties in the corresponding reduction potentials. It is therefore concluded that the calculated reduction potentials may very well be compatible with the experimental observations, as well as those suggested in Ref. [3]. In particular, in combination with the proton pumping observations, it should be possible to conclude that the energy profile obtained here from the calculations most likely is closer to the truth than the red profile in Fig. 7.

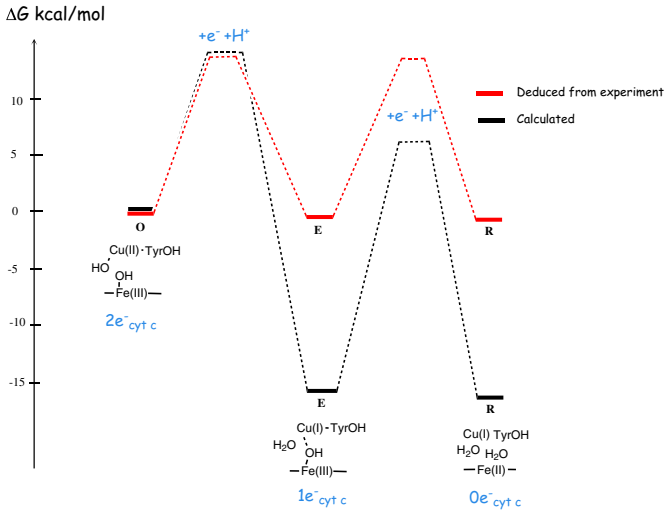

Fig. 7. Estimated free energy profile for the resting states in the reductive part of the catalytic cycle of CcO, comparing calculated and experimental results. The black curve is obtained from the present calculations as described in the text. The red curve is obtained using the experimentally deduced reduction potentials for Cu_B and heme a_3 [3]. The blue notation $2e^-_{cytc}$ represents two equivalents ferrocytochrome c used in the equilibrium experiments [3].

Thus, the calculations show that the reduction potential of Cu_B seems to be significantly larger than previously estimated on the basis of experiment, which explains why proton pumping can occur in at least one of the two reduction steps considered to be problematic. The exact value of the Cu_B potential is determined by several factors. Already for the separate copper complex, the calculated reduction potential of 0.64 V (see Table 1) is larger than the values suggested for CcO by experiments, 0.28–0.35 V [2,3] (see Table 2). The presently calculated reduction potential involves the chemistry of water formation, which makes it different from many other copper protein cofactors. It should also be remembered that the reduction potential for Cu(II) is known to vary substantially in proteins, e.g. for the blue copper proteins values between 0.3 and 0.8 V are found [23]. As shown in Table 1 the Cu(II) potential increases even further in the combined BNC model, to 0.95–1.06 V, depending on the stage in which the reduction occurs. The calculated potential for the actual **O** to **E** transition in Fig. 7 is 0.95 V, and the increase compared to the isolated copper complex is partly due to an increase in the binding energy of the water molecule just formed, which has a strong hydrogen bond to the hydroxyl group on iron. It is also due to a direct interaction between the two parts of the BNC, which results in a short distance between copper and the hydroxyl group on iron in **E**, see Fig. S7.

On the other hand, the calculations indicate that the Fe(III) reduction potential actually has a low value, as expected from experiment. Therefore another important feature of the reaction mechanism described in Fig. 4 may explain the observed proton pumping in the second problematic reduction step, namely the presence of an alternative to the very low lying state **E**, the metastable state $\mathbf{E}_H$. It turns out that the appearance of the tyrosyl radical in several intermediates plays an important role, in particular in the two metastable states $\mathbf{O}_H$ and $\mathbf{E}_H$. The energetic position of the $\mathbf{E}_H$ state, not too low, but also not too high, makes it possible to distribute the free energy more equally over the two reduction steps in the reductive part of the catalytic cycle. The $\mathbf{O}_H$ to $\mathbf{E}_H$ transition is mainly described as a reduction of Fe(III)OH to Fe(II)-OH_2. However, the electronic structure of the $\mathbf{E}_H$ state, as reflected in the spin population (see Fig. S3), reveals that it is not a pure Fe(II) state, but there is a slight involvement of an Fe(III) state, which is obtained by a partial electron transfer from iron to the tyrosyl radical. Thus the $\mathbf{E}_H$ state can be viewed as a mixture of two electronic structures: $TyrO^{\bullet}$–Fe(II)-OH_2 (main) and $TyrO^{-}$–Fe(III)-OH_2 (minor). This mixture of electronic states is necessary for an optimal energy level of this state, and it is made possible by the presence of the tyrosyl radical in the main configuration. The involvement of the Fe(III) state is also reflected in the stronger binding of the water molecules in the $\mathbf{E}_H$ state as compared to both the $\mathbf{E}_R$ and the **R** states, which have to be pure Fe(II) states since there is no tyrosyl radical present that can accept some electron transfer from iron. The $\mathbf{O}_H$ to $\mathbf{E}_H$ ($TyrO^{\bullet}$–Fe(II)-OH_2) transition, where the main reduction process is Fe(III)OH to Fe(II)-OH_2, has a calculated exergonicity of 8.1 kcal/mol, see Fig. 6. If the same reduction occurs in the **E** to **R** (TyrOH–Fe(II)-OH_2) transition, it has a much smaller calculated exergonicity (less than 3 kcal/mol). This difference is, thus, due to a slight mixing with tyrosyl reduction in the first case, which is possible due to the presence of the tyrosyl radical. If these reduction energies are transformed into midpoint potentials (including proton uptake), see Table 1, the pure Fe(III)OH to Fe(II)-OH_2 reduction in the **E** to **R** transition gives a value of 0.37 V. This value is slightly smaller than the value of 0.48 V for the separated heme complex, which is caused by a stabilization of the Fe(III)OH reactant in the BNC, due to the interaction between the copper ion and the hydroxyl oxygen. The BNC value

of 0.37 V is also close to the experimentally expected range in CcO of 0.29–0.35 V [2,3] (see Table 2). On the other hand, the $\mathbf{O}_H$ to $\mathbf{E}_H$ transition corresponds to the larger midpoint potential of 0.60 V, due to some mixing with the larger tyrosyl reduction potential. A consequence of the mechanism suggested here is clearly that the reduction of the tyrosyl radical actually occurs in the reductive part of the catalytic cycle. The midpoint potential for tyrosyl reduction obtained from the $\mathbf{E}_H$ to **R** transition is quite low, 0.55 V, which is partly due to the mixing with the smaller Fe(III) reduction potential from the previous step as just discussed. Table 1 shows that there is also a small decrease in the tyrosyl midpoint potential going from the separated copper–tyrosine complex (0.86 V) to the BNC model (0.55–0.77 V). This decrease of the tyrosyl potential in the BNC seems to be caused by a stabilization of the tyrosyl radical reactant by the hydrogen bonding to the farnesyl group, which causes a slight electron transfer to the tyrosyl radical, as indicated by the spin populations.

Finally, to ensure the involvement of the metastable $\mathbf{E}_H$ state during catalytic turnover, there must be a mechanism to avoid the low energy trap, the **E** state, which means that the proton must be prevented by high enough barriers from reaching the tyrosinate. Obviously, if the proton is transferred in the K-channel, protonation of the tyrosinate cannot be avoided. It is therefore suggested here, that the barrier in the K-channel, at least at this point of the reaction, is higher than the barrier in the D-channel, such that the proton uptake in the first reduction step in the reductive part of the catalytic cycle occurs via the D-channel, see further above. Thus, it is suggested that only a single proton is taken up via the K-channel under catalytic turnover, which is in contrast to the interpretation of some experimental information suggesting that two protons are taken up to the BNC via the K-channel. Furthermore, a proton may not be allowed to move from the water molecules in the BNC to the tyrosinate after the $\mathbf{E}_H$ state has been formed, which would also lead to the low energy **E** state. Preliminary calculations using a larger model indicate that the barrier for such a proton motion is indeed quite high at this point in the catalytic cycle. One reason for a high barrier at this stage is that there is a quite large energy cost for the rearrangement required at the iron center, going from high spin Fe(II) with loosely coordinated water molecules, to an Fe(III)OH state. Thus, an important conclusion from the present study is that to avoid the low energy **E** state for the one electron reduced intermediate, there has to be a high barrier in the K-channel at this point.

A few words should also be said about the reduction potentials in the oxidative part of the catalytic cycle. As already discussed, the calculations give a quite large reduction potential for the Cu(II)OH to Cu(I)-OH_2 reduction, 0.64 V for the separate copper complex, which increases to 0.95–1.06 V in the BNC model, see Table 1. A large part of the explanation for this increase is that the water molecule formed in this reduction step has a larger binding energy in the BNC as compared to the separate copper complex. The largest midpoint potential of 1.06 V for the copper reduction is actually obtained for the $\mathbf{P}_M$ to **F** transition, where the water molecule forms a stronger hydrogen bond to the ferryl-oxo group than the reactant hydroxyl group. The spin populations indicate that the electrons in the Fe(IV)═O double bond are shifted towards the oxygen due to the interaction with the positive charge of the water proton (see Figs. S5–S6). There is also a contribution to the high copper reduction potential from direct interaction between the positively charged Cu(I)-ion and the Fe(IV)═O complex, resulting in a short Cu – O distance in the reduced product. As shown in Fig. 4, in the mechanism suggested by the calculations the copper reduction actually occurs as the first step after the O – O bond cleavage, i.e. in the $\mathbf{P}_M$ to **F** transition. In the next step, the **F** to **O** transition, or rather the **F** to $\mathbf{O}_H$, Fe(IV)═O is reduced to Fe(III)OH. The calculated midpoint potential (including both electron and proton uptake) for this reduction is slightly larger in the BNC model, 0.82 V, as compared to 0.72 V in the separate heme complex. The increase is caused by an interaction between the copper ion and the hydroxyl group in the $\mathbf{O}_H$ product, resulting in a rather short distance between copper and the hydroxyl oxygen (see Fig. S2). Interestingly, these calculated midpoint potentials of 1.06 V and 0.82 V for the first two reduction steps after O_2 cleavage agree well with the corresponding experimental values, 0.82–1.20 V, and 0.76–1.05 V, respectively [2,4] (see Table 2).

2.3. Proton pumping at high electrochemical gradient

In contrast to the expectations based on experimental reduction potentials, the calculated energy profile discussed in the previous sections shows that all four reduction steps in the catalytic cycle of A-family CcOs are exergonic. However, the exergonicities in the reductive part of the cycle are smaller than those in the oxidative part, 7–8 kcal/mol per reduction step, as compared to 13–19 kcal/mol in the oxidative part. When the gradient increases the exergonicity decreases in all reduction steps, due to charge motion against the gradient. It can therefore still be questioned if the calculated energetics are compatible with full proton pumping also at a high gradient. In the present section, the requirements for proton pumping at high gradient are discussed.

The energy profile presented in the Section 2.1 above can be used as a starting point, but to discuss the energetic requirements for proton pumping in the different parts of the catalytic cycle the rate limiting proton transfer barriers have to be included. This means that the energy profile has to be simplified in some other aspects. The black curve in Fig. 8 shows the calculated energy profile discussed above, but with each reduction step shown as a single step, including both electron and proton transfer. All barriers, including now also the pumped protons, in each reduction step are condensed into a single barrier for the entire reduction step. The height of these rate limiting barriers is estimated from experimental data, and they are put to 13 kcal/mol, corresponding to rates on the millisecond time scale, see Section A.3 in Appendix A. Furthermore, the orange curve in Fig. 8 describes the situation when the electrochemical gradient has reached 85% of the maximum value. Since both the electrogenic chemistry and the proton pumping correspond to moving charges against the gradient, all these elementary steps contribute to making the reaction less exergonic. It is also expected that the charge transfer barriers increase somewhat with the gradient present, which is also included in the orange energy profile. Se Section A.3 in Appendix A for details.

In most experiments investigating proton pumping a situation without any significant gradient is considered. Without gradient there is no cost for the proton pumping, which means that even endergonic individual reduction steps could be coupled to proton pumping, as long as there is a driving force from subsequent exergonic reduction steps. However, recent interpretations of the experimental data on ATP production in mitochondria indicate that, also at a significant gradient the pumping stoichiometry is fairly high [5,6]. The gradient value of 170 mV (85% of the maximum value 200 mV) in Fig. 8 was chosen to possibly represent this experimental situation. Interestingly, the orange curve in the figure shows that all reduction steps but one (the $\mathbf{E}_H$ to **R** transition) are still exergonic with this gradient present. Furthermore, the one exception (the $\mathbf{E}_H$ to **R** transition) is followed by exergonic steps not affected by the gradient (O_2 binding and cleavage). Altogether, this means that there is no endergonicity added to the rate determining barriers in any reduction step, and the reaction rate is still determined by the local barrier heights. Thus full proton pumping would not slow down the reaction at this gradient more than from the direct effect on the proton transfer barriers. However, it must be noted that when the gradient increases the difference in barrier height decreases between the reaction paths leading to proton pumping and those leading to leakage, which means that the proton pumping must become less efficient.

3. Comment on the reliability of the computational results and comparison to previously published results

As noted already in the introduction, the present type of computational investigation is very challenging, and many conclusions drawn

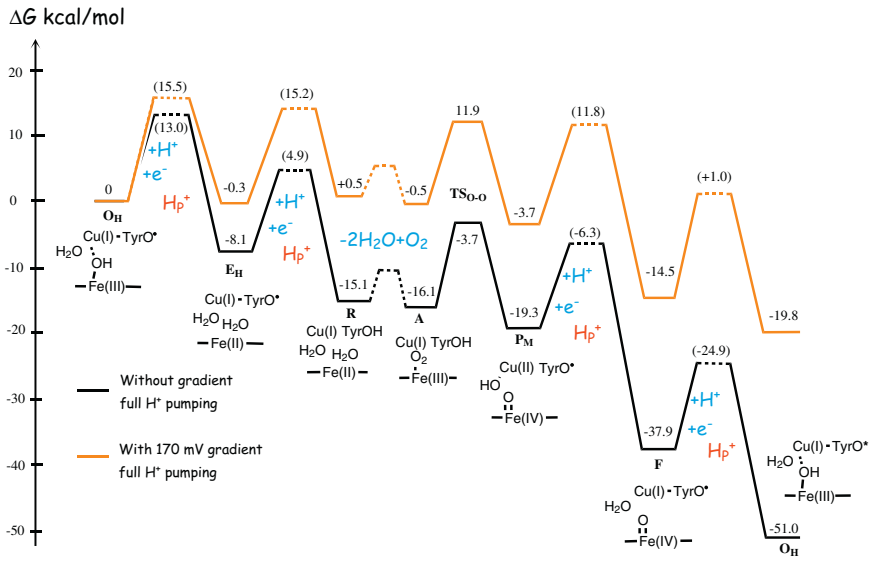

Fig. 8. Calculated free energy profile for the catalytic cycle of CcO, black curve. The orange curve corresponds to the situation with 85% of the maximum gradient present. The procedure used to add the energetic effects of the gradient is described in the text, and a more detailed description is given in Section A.3 in Appendix A. The notation H_P^+ corresponds to pumped protons.

in this study are not based solely on the computational results, but rather on a combination of calculated and experimental results. Clearly, this raises the question whether one could use the computational results to draw also different conclusions. Therefore this section is used to try to evaluate and explain the reliability in the results used to draw the various conclusions. As will be shown, the properties that are most difficult to calculate are connected to the heme-iron. In particular, comparisons to high accuracy calculations (coupled cluster (CCSD(T))) [24–26] have shown that lower spin states for iron are too stable relative to higher spin states in B3LYP* (and B3LYP) calculations on small porphyrin models. As described above, the calculated reduction potentials listed in Table 1 are obtained by adjusting the overall reaction energy for one catalytic cycle to the value obtained from experimental reduction potentials of the donor and the acceptor, while the *relative* reduction potentials are independent of this adjustment to experiment. Thus, the relative values are obtained directly from the calculations, and therefore they are used in the discussion below.

The most important conclusion in the present study, that Cu_B has a fairly high charge compensated reduction potential (electron plus proton), is a result that emerges directly from the calculations, and which turns out to be quite stable to both models and methods. A rough conclusion from Table 1 is that the Cu(II) potential is of a similar magnitude as the potentials of the tyrosyl radical and the ferryl group. Already for the separate copper complex, the Cu(II) potential is only about 0.2 V smaller than that for the tyrosyl radical. Going to the BNC model, the Cu(II) potential increases by 0.3–0.4 V from hydrogen bonding and direct interaction with the iron complex, while the tyrosyl potential decreases slightly, with the result that the Cu(II) potential is even larger than the tyrosyl potential in the BNC. (Note that the very low value of 0.55 V listed in Table 1 is not a pure tyrosyl reduction, as discussed in Section 2.2 above.) Furthermore, a smaller model of the copper-complex with only pure imidazole ligands, gives the same value for the O–H bond strength as the larger model taken as a part of the BNC-model. More importantly, this smaller model gives almost identical results for B3LYP* (and B3LYP) and the more reliable CCSD(T) method [27]. Therefore, it seems quite safe to conclude that Cu_B has a reduction potential of similar size as, or even larger than, the tyrosyl radical, and possibly also rather similar to the ferryl group (see further below). It is noted that the calculated tyrosyl O–H bond strength, used to determine the charge compensated reduction potential for the tyrosyl radical, agrees very closely with the expected experimental value, as can be estimated from experimental results for phenols with substituents in the orto and para positions [28].

As mentioned above, the reduction potentials that are most difficult to calculate, are the two involving heme a_3, the Fe(IV)═O and the Fe(III) potentials. Still, it is quite clear that the calculations support the low charge compensated Fe(III) reduction potential obtained for heme a_3 in equilibrium experiments. The very good agreement between the calculated value for the BNC-model, 0.37 V, and the experimental values, 0.29–0.35 V [2,3], must be considered fortuitous, though, in particular considering that the calculated value involves a large correction of 7.6 kcal/mol, which depends on the calculated binding energy of molecular oxygen to the reduced BNC. An indication of the uncertainty in a calculated property is that different DFT-functionals, such as B3LYP* and B3LYP, give different results. If the B3LYP functional was used instead of B3LYP*, the corresponding correction would be only 1.1 kcal/mol. The corresponding reduction potential would then be 0.14 V, which is not very far either from the experimental range, 0.29–0.35 V. Finally, the uncertainty in the calculated charge compensated reduction potential for Fe(IV)═O is mainly connected to the difficulty in calculating correct spin-splittings. As was mentioned above, this problem is illustrated by CCSD(T) calculations on small heme-model, and it is also indicated by differences between the results from the two functionals B3LYP* and B3LYP. An estimate of the uncertainty in the reported potential for Fe(IV)═O of 0.82 V given in Table 1, can be obtained by considering the range of values obtained for either high spin or low spin Fe(III) using either the B3LYP* or the B3LYP functional. The range of values thus obtained, 0.82–1.17 V, is quite close to the experimental range, 0.76–1.05 V [2,4]. It can be concluded that the uncertainty in the calculated reduction potentials for heme a_3 seems to be similar to the uncertainty in the experimental values, and also that the calculated and the experimental potentials are quite similar. It was chosen here to report the B3LYP* results, because this functional is generally considered to give better results for transition metal systems [29], but these results also give an overall picture that agrees somewhat better with other experimental information, such as the proton pumping at high gradient in all four reduction steps. To obtain the present picture it is also important to use the high-spin iron states for several intermediates, although they are in some cases not the states with the lowest calculated energy. This is a difference to previously published results, e.g. [10,30]. Another difference compared to previous studies is that there are no extra water molecules in the present BNC

model. The exclusion of water molecules turned out to generate more well defined electronic structures of the intermediates in the catalytic cycle.

Another important conclusion of the present study is that only one proton is taken up via the K-channel during catalytic turnover, to avoid the low energy of the one electron reduced **E** state, which has a protonated tyrosine. This conclusion is directly connected to the low reduction potential of the Fe(III) state, and as seen above this is a stable result, independent of the method used. The low energy of the tyrosine structure for the one electron reduced intermediate was observed already in the previously published calculations [10,30]. Therefore it was suggested already then that the tyrosine should stay unprotonated until the BNC became fully reduced, to leave enough energy for proton pumping in the second reduction step [10,30]. However, in the previous publications, no conclusions were drawn, based on the calculations, regarding the number of protons transferred via the K-channel. Furthermore, a previous discussion on the pumping mechanism assuming the uptake of two protons via the K-channel [14], was based on the conclusions drawn by experimental researchers.

4. Conclusions

The mechanism for reduction of molecular oxygen to water in cytochrome c oxidase (CcO) has been studied using quantum chemical calculations (hybrid density functional theory). The model of the BNC used in the calculations, based on a crystal structure for an A-family CcO [16], has about 140 atoms. By adding electrons and protons separately all intermediates in the reduction process are studied. The reduction mechanism appearing from these calculations suggests that the tyrosyl radical plays a role in several reduction steps, see Fig. 4. More importantly, the corresponding calculated free energy profile shows that all four reduction steps have enough exergonicity to afford proton pumping also with a significant gradient present, in agreement with experimental observations [5,6]. The calculations show that three of the four reduction potentials involved in the reduction process are of similar magnitude, and large enough to yield a substantial exergonicity for electron transfer from the donor cytochrome c, namely the potentials for the tyrosyl radical, the ferryl group (Fe(IV)═O) and Cu_B (Cu(II)). The high charge compensated reduction potential for Cu(II) obtained from the calculations is in contrast to the experimental equilibrium estimates, indicating a very low potential for Cu(II) [3]. It is noted here that the uncertainty in estimated amounts of reduced copper, due to lack of direct methods, makes it very difficult to determine the Cu(II) potential from this type of equilibrium experiments, making the reported experimental value very uncertain. It is therefore argued that the calculated high value should be more reliable, in particular since the experimentally estimated low value is in conflict with the observations of proton pumping in all four reduction steps. The calculated Fe(III) potential, on the other hand, agrees with the low value obtained from the equilibrium experiments [3].

The calculations furthermore suggest that the so called metastable states, $\mathbf{O}_H$ and $\mathbf{E}_H$, involved in the catalytic reaction cycle, both have a tyrosyl radical, while the corresponding resting states **O** and **E** are suggested to have a protonated tyrosine. In contrast to what has been experimentally suggested, the $\mathbf{O}_H$ state does not have significantly higher energy than the **O** state. Instead, a large energy difference is obtained between the $\mathbf{E}_H$ and **E** states. The presence of the high energy $\mathbf{E}_H$ state explains how both reduction steps $\mathbf{O}_H$ to $\mathbf{E}_H$ and $\mathbf{E}_H$ to **R** can be exergonic enough to allow proton pumping with a gradient, in spite of the low reduction potential for the Fe(III) state. The $\mathbf{E}_H$ state turns out to be a mixture of states, leading to a small amount of electron transfer from iron to the tyrosyl radical. Thus, the role of the $\mathbf{O}_H$ state is not to provide a larger exergonicity for the **O** to **E** transition, as previously suggested, but rather to prepare for the formation of the $\mathbf{E}_H$ state. To secure the involvement of the $\mathbf{E}_H$ state in the catalytic reaction, it has to be assumed that only a single proton is taken up via the K-channel during turnover, namely the one that protonates the tyrosine in the $\mathbf{E}_H$ to **R** step. It is argued that it is a reasonable assumption that the barrier in the D-channel, for proton uptake to the BNC, is lower than the barrier in the K-channel for all reduction steps except the $\mathbf{E}_H$ to **R** step. In the $\mathbf{E}_H$ to **R** step the oxygen ligands on the metal ions in the BNC are fully protonated, which should yield a high barrier for proton uptake to the tyrosine via the D-channel. Furthermore, it has to be assumed that the barrier for internal proton motion from the central BNC to the tyrosine residue is fairly high, at least in the $\mathbf{E}_H$ state. Preliminary calculations using a larger model indicate that this indeed is the case. Otherwise it should be noted that no barriers are studied with the present model, and all explicit barriers used in the discussion of the results are estimated on the basis of experimental results.

Finally, a comment can be made about proton pumping in the B- and C-family CcOs. These enzymes have only one channel for proton uptake from the N-side, located at a similar position as the K-channel in the A-family CcOs. Clearly, when all chemical protons are forced to be taken up via the K-channel analogue (passing through the redox active tyrosine) it is not possible to avoid the low energy **E** state during catalytic turnover, and the metastable $\mathbf{E}_H$ state with an unprotonated tyrosine will never be formed. Therefore the second step in the reductive part of the cycle will have a very low (or zero) exergonicity already without the gradient, which means that proton pumping in this step, if it at all occurs, should be very sensitive to the presence of the gradient for CcOs belonging to the B- and C-families. It is also known that the total free energy available for all four reduction steps is smaller for the B- and C-families, since molecular oxygen binds much stronger in these enzymes, as compared to the A-family [31,32]. These two facts, the lack of the $\mathbf{E}_H$ state and the lower energy available, probably explain the difficulties to obtain agreement regarding the maximum number of protons pumped in the B- and C-family CcOs, and also the suggested larger sensitivity of the proton pumping to the presence of the gradient [32–34].

Acknowledgments

We are grateful to Peter Brzezinzki and Mårten Wikström for valuable discussions.

Appendix A. Models and methods

Quantum chemical calculations have been performed on a model of the BNC in the A-family CcO to obtain a detailed description of the catalytic cycle. In the first subsection below the model of the BNC used in the calculations is described, and in the second one the quantum chemical methods are described. In the final subsection the procedure used to connect the calculated relative energies to experimental data is described.

A.1. Model of the BNC

The binuclear active site (BNC) in the A-family CcOs consists of a high-spin heme a_3 group in close vicinity of a histidine ligated copper complex (Cu_B). The model used in the calculations is based on a high resolution crystal structure from *Rhodobacter sphaeroides* [16], see Fig. 3. The heme a_3 part of the BNC is modeled by a heme a, keeping the substituents except the 15-carbon farnesyl chain and the two propionate groups, which are replaced by hydrogen atoms. The proximal histidine is included. Larger models of the heme group, e.g. including the propionate groups, together with their hydrogen bonding arginine residues, have been found to give similar results [10]. The Cu_B model includes the three histidine ligands together with the cross-linked tyrosine. The amino acids are truncated at the alpha-carbon, which is fixed to the X-ray coordinates during geometry optimizations to maintain some of the constraints from the surrounding protein. The peptide bonds are replaced by C–H bonds, with the hydrogen atoms fixed.

One carbon atom on the porphyrin is also fixed. No water molecules, apart from the ones formed during the reduction process, are included in the model (see further below). The model constructed in this way has about 140 atoms (depending on the state).

Using the model shown in Fig. 3 the different intermediates in the catalytic cycle are constructed by adding molecular oxygen, electrons and protons in separate steps. This means that for each reduction step illustrated in Fig. 2, two intermediates are considered, one with only an electron added, and one with both an electron and a proton. For each intermediate, different states are investigated, both with respect to the location of the protons and electrons, and with respect to the spin-coupling. For the location of the proton, there are essentially two possibilities, either the proton is placed on one of the oxygens in the actual BNC or it is placed on the tyrosyl oxygen which was deprotonated in the O – O bond cleavage step. These different structures for the intermediates are discussed in the results section. For the spin-states, the main issue regards the spin-state of the iron ion, while the spin-coupling between the different parts of the active site turns out be unimportant for the energy. Normally, the spin-state for which the calculations give the lowest energy is reported, but it has been shown that density functional theory does not give correct spin-splittings for heme-models [14,24–26]. In particular it was shown that the DFT functionals used here stabilize lower spin states for iron too much relative to the higher spin states. Therefore, some corrections have to be introduced here. Based on experimental information heme a_3 is generally considered to have a high-spin iron, and therefore the energy of the high-spin iron states is reported for most intermediates. The main exceptions are the Fe(IV)═O complexes and the ferric superoxo complex, where the states reported have low-spin iron, which have the lowest energy in the calculations. Furthermore, for the high-spin ferrous state a correction is introduced, lowering this state by 7.6 kcal/mol, to give agreement with the experimental binding energy of molecular oxygen in the **A** intermediate [17].

Another aspect of the model used in the calculations concerns possible water molecules in the BNC. Several X-ray structures contain a few water molecules inside and close to the BNC. Since water is formed during the reduction process, it is likely that some of them stay within or in the vicinity of the BNC. However, different X-ray structures have different numbers of and positions for the water molecules. Furthermore, it is very difficult to use calculations to determine the optimal number of and positions for water molecules in the BNC. Therefore, it was decided to use a model without any water molecules, except the ones formed in the reaction, at the present stage. This means that the calculations describe the basic chemistry occurring during the reduction process, with "intrinsic" relative energies. Clearly, addition of water molecules in the BNC might modulate the energetics and the charge distribution slightly, but should not change the general picture. An important aspect is that this model without any "extra" water molecules is only used to calculate these intrinsic reaction energies. Neither proton motion nor transition states are studied using this model. As will be discussed below, all barrier heights presented in this study are obtained from experimental rates.

A.2. Computational methods

Quantum mechanical calculations were performed on the BNC model employing the dispersion corrected hybrid density functionals B3LYP-D3 [35,36] and B3LYP*-D3 [29], the latter using 15% Hartree–Fock exchange instead of 20% as used in the original functional. All structures were fully optimized, except for some atoms fixed from the crystal structure as mentioned above, using the B3LYP-D3 functional and the basis set labeled lacvp* in the Jaguar program [37], which is a double zeta basis with polarization functions on all second row atoms. Single point calculations were performed in the optimized structures using the large cc-pvtz(-f) basis set plus lacv3p+ for the metal ions with both the B3LYP-D3 and the B3LYP*-D3 functional. Solvent effects from the surrounding protein were included using the self consistent reaction field (SCRF) approach as implemented in Jaguar with a dielectric constant of 4.0, in accordance with previous experience [38]. The dielectric calculations were performed for the optimized structures using the B3LYP-D3 functional and the lacvp* basis set. The program Jaguar 7.6 [37] was used in all calculations described so far.

In all optimized structures the Hessian matrix, i.e. second derivatives of the energy with respect to the nuclear coordinates, was calculated using the Gaussian 09 package [39] at the same level of calculation as the geometry optimizations (B3LYP-D3/lacvp*). The Hessians were used to calculate zero-point corrections, but due to the fixed coordinates in the geometry optimizations, entropy effects would not be reliable and could not be taken from the Hessian calculations. The entropy changes within the BNC itself are assumed to be small and therefore neglected. The main entropy changes occur when molecules enter or leave the system, and these have to be estimated in some approximate way. For the gaseous O_2 molecule it is assumed that the entropy lost on binding is equal to the translational entropy for the free molecule (10.8 kcal/mol at room temperature). For the binding of a water molecule to bulk water a standard value of 12 kcal/mol is used, which includes explicit zero point effects for the water molecules.

The relative energies reported are referred to as free energy values, with entropy effects estimated as described in the previous paragraph. The enthalpy values are obtained from the large basis set calculations using the B3LYP*-D3 functional, including zero point and solvent effects. Using the B3LYP-D3 results instead of B3LYP*-D3 gives a similar picture.

A.3. Overall energetics, barriers and effects of the gradient

To obtain an energy diagram for the full catalytic cycle of CcO the energetics of the reduction steps has to be calculated, which means that the cost for the uptake of electrons and protons from the donors has to be estimated. Since it is not possible to calculate accurate absolute reduction potentials, a procedure is used where the overall energy of one catalytic cycle is adjusted to the value obtained from experimental reduction potentials [9–12,15,40]. Using experimental values of 0.25 V for the electron donor cytochrome c, and 0.8 for the electron acceptor, O_2 forming water, the exergonicity of one catalytic cycle of CcO becomes 51.0 kcal/mol (2.2 V) [1]. In combination with the calculated free energy for the chemistry occurring in Eq. (1), the cost of each reduction step (transfer of one electron from cytochrome c and one proton from the bulk) becomes 67.8 kcal/mol, to yield the total experimental exergonicity of 51 kcal/mol. Together with the calculated energies of the intermediates, this determines the relative energies for each of the reduction steps in the catalytic cycle. However, this procedure does not give the individual costs for the electron and the proton, and therefore there is one parameter left to be determined in some other way. In the present case, this parameter is chosen to fit certain experimental information about the reduction process. The rate of electron transfer to the BNC is known to be slightly dependent on the presence of a positively charged lysine in the K-channel. Since this lysine is not included in the present model, the parameter is chosen to make the electron transfer to the **F** state, which has one of the lowest calculated electron affinities, slightly endergonic. This choice of the parameter, furthermore, makes the second electron transfer in the reductive part of the cycle quite endergonic, which also is in agreement with experimental observations that this reduction step does not occur without the lysine in the K-channel. Finally, with this parameter choice, the electron transfer in the remaining two reduction steps becomes slightly exergonic, which is reasonable.

The main part of the present study concerns the thermodynamics of the different reduction steps. Therefore the barriers for the transitions between states play a minor role. Each reduction step involves several elementary steps of electron and proton (both chemical protons (to the BNC) and pumped protons) transfer. It is expected that the transfer of the pumped protons is rate limiting for each reduction step. In the calculated energy profile describing both electron and proton transfer

states, the transfer of the pumped protons is not included. In this energy profile the barriers for electron and proton transfer (to the BNC) are just indicated as fairly low, since they are not rate limiting. However, in the discussion about proton pumping at a high gradient, kinetics has to be taken into account. Therefore, an energy profile is constructed where each reduction step is described in a simplified way with a single rate limiting barrier. The reaction rates for the different reduction steps are known to be in the 100 to 1000 μs range, and the same approximate value of 13.0 kcal/mol, without gradient, is used in all reduction steps for the rate limiting barrier. For the O – O bond cleavage barrier, an accurate value of 12.4 kcal/mol [18], is obtained from experiment, deduced from the life-time of compound **A** using transition state theory.

The presence of the electrochemical gradient across the membrane will affect both the relative energies of the intermediates in the CcO reaction, and the barrier heights. The intermediates are affected since the movement of charge against the gradient is endergonic, in contrast to the situation without gradient, where there is no thermodynamic cost connected with the movement of the charges from one side of the membrane to the other. In the present study the effect of a gradient of 170 mV, i.e. 85% of its maximum value of 200 mV [1], is investigated. This means that an extra cost of 3.9 kcal/mol is added for each charge moved against the gradient across the membrane. Thus the effects of the gradient on the relative energies of the intermediates can easily be estimated, since only charge transfer steps across the entire membrane need to be considered at the present level of detail in the analysis. The effect of the gradient on the rate limiting charge transfer barrier depends on the particular mechanisms involved in the charge movement. Here the rate limiting barrier is increased by 2.5 kcal/mol at a gradient of 170 mV.

Appendix B. Supplementary data

Supplementary data to this article can be found online at http://dx.doi.org/10.1016/j.bbabio.2014.12.005.

References

[1] P. Brzezinski, Redox-driven membrane-bound proton pumps, Trends Biochem. Sci. 29 (2004) 380–387.
[2] G.T. Babcock, M. Wikström, Oxygen activation and the conservation of energy in cell respiration, Nature 356 (1992) 301–309.
[3] D. Jancura, V. Berka, M. Antalik, J. Bagelova, R.B. Gennis, G. Palmer, M. Fabian, Spectral and kinetic equivalence of oxidized cytochrome c oxidase as isolated and "activated" by reoxidation, J. Biol. Chem. 281 (2006) 30319–30325.
[4] V.R.I. Kaila, M.I. Verkhovsky, M. Wikström, Proton-coupled electron transfer in cytochrome oxidase, Chem. Rev. 110 (2010) 7062–7081.
[5] S.J. Ferguson, ATP synthase: from sequence to ring size to the P/O ratio, Proc. Natl. Acad. Sci. U. S. A. 107 (2010) 16755–16756.
[6] M. Wikström, G. Hummer, Stoichiometry of proton translocation by respiratory complex I and its mechanistic implications, Proc. Natl. Acad. Sci. U. S. A. 109 (2012) 4431–4436.
[7] M.I. Verkhovsky, A. Jasaitis, M.L. Verkhovskaya, J.E. Morgan, M. Wikström, Proton translocation by cytochrome c oxidase, Nature 400 (1999) 480–483.
[8] D. Bloch, I. Belevich, A. Jasaitis, C. Ribacka, A. Puustinen, M.I. Verkhovsky, M. Wikström, The catalytic cycle of cytochrome c oxidase is not the sum of its two halves, Proc. Natl. Acad. Sci. U. S. A. 101 (2004) 529–533.
[9] P.E.M. Siegbahn, M.R.A. Blomberg, M.L. Blomberg, A theoretical study of the energetics of proton pumping and oxygen reduction in cytochrome oxidase, J. Phys. Chem. B 107 (2003) 10946–10955.
[10] M.R.A. Blomberg, P.E.M. Siegbahn, Quantum chemistry applied to the mechanisms of transition metal containing enzymes — cytochrome c oxidase a particularly challenging case, J. Comp. Chem. 27 (2006) 1373–1384.
[11] P.E.M. Siegbahn, M.R.A. Blomberg, Modeling of Mechanisms for Metalloenzymes Where Protons and Electrons Enter or Leave, in: K. Morokuma, J. Musaev (Eds.), Computational Modeling for Homogeneous Catalysis and Biocatalysis, Wiley-VCH, Germany, 2008, pp. 57–81.
[12] P.E.M. Siegbahn, M.R.A. Blomberg, Quantum chemical studies of proton-coupled electron transfer in metalloenzymes, Chem. Rev. 110 (2010) 7040–7061.
[13] M.R.A. Blomberg, T. Borowski, F. Himo, R.-Z. Liao, P.E.M. Siegbahn, Quantum chemical studies of mechanisms for metalloenzymes, Chem. Rev. 114 (2014) 3601–3658.
[14] M.R.A. Blomberg, P.E.M. Siegbahn, Proton pumping in Cytochrome c oxidase: energetic requirements and the role of two proton channels, Biochim. Biophys. Acta 1837 (2014) 1165–1177.
[15] P.E.M. Siegbahn, Water oxidation mechanism in photosystem II, including oxidations, proton release pathways, O – O bond formation and O_2 release, Biochim. Biophys. Acta 1827 (2013) 1003–1019.
[16] L. Qin, C. Hiser, A. Mulichak, R.M. Gavarito, S. Ferguson-Miller, Identification of conserved lipid/detergent-binding sites in a high-resolution structure of the membrane protein cytochrome c oxidase, Proc. Natl. Acad. Sci. U. S. A. 103 (2006) 16117–16122.
[17] M.I. Verkhovsky, J.E. Morgan, M. Wikström, Oxygen binding and activation in the reaction of oxygen with cytochrome c oxidase, Biochemistry 33 (1994) 3079–3086.
[18] M. Karpefors, P. Ädelroth, A. Namslauer, Y. Zhen, P. Brzezinski, Formation of the "peroxy" intermediate in cytochrome c oxidase is associated with internal proton/hydrogen transfer, Biochemistry 39 (2000) 14664–14669.
[19] M. Bränden, H. Sigurdson, A. Namslauer, R. Gennis, P. Ädelroth, P. Brzezinski, On the role of the K-proton transfer pathway in cytochrome c oxidase, Proc. Natl. Acad. Sci. U. S. A. 98 (2001) 5013–5018.
[20] K. Ganesan, R.B. Gennis, Blocking the K-pathway still allows rapid one-electron reduction of the binuclear center during the anaerobic reduction of the aa_3-type cytochrome c oxidase from *Rhodobacter sphaeroides*, Biochim. Biophys. Acta 1797 (2010) 619–624.
[21] V. Sharma, K.D. Karlin, M. Wikström, Computational study of the activated O_H state in the catalytic mechanism of cytochrome c oxidase, Proc. Natl. Acad. Sci. U. S. A. 110 (2013) 16844–16849.
[22] B.F. Van Gelder, H. Beinert, Studies of the heme components of cytochrome c oxidase by EPR spectroscopy, Biochim. Biophys. Acta 189 (1969) 1–24.
[23] H.B. Gray, B.G. Malmsöm, R.J.P. Williams, Copper coordination in blue proteins, J. Biol. Inorg. Chem. 5 (2000) 551–559.
[24] M. Radon, K. Pierloot, Binding of CO, NO, and O_2 to heme by density functional and mulitireference ab initio calculations, J. Phys. Chem. A 112 (2008) 11824–11832.
[25] S. Vancoillie, H. Zhao, M. Radon, K. Pierloot, Performance of CASPT2 and DFT for relative spin-state energetics of heme models, J. Chem. Theory Comput. 6 (2010) 576–582.
[26] J. Olah, J.N. Harvey, NO bonding to heme groups: dft and correlated av initio calculations, J. Phys. Chem. A 113 (2009) 7338–7345.
[27] K. Pierloot, Q. M. Phung, private communication [2014].
[28] M. Lucarini, P. Pedrielli, G.F. Pedulli, Bond dissociation energies of O – H bonds in substituted phenols from equilibration studies, J. Org. Chem. 61 (1996) 9259–9263.
[29] M. Reiher, O. Salomon, B.A. Hess, Reparameterization of hybrid functionals based on energy differences of states of different multiplicity, Theor. Chem. Accounts 107 (2001) 48–55.
[30] P.E.M. Siegbahn, M.R.A. Blomberg, The combined picture from theory and experiments on water oxidation, oxygen reduction and proton pumping, Dalton Trans. (2009) 5832–5840.
[31] I. Szundi, C. Funatogawa, J.A. Fee, T. Soulimane, O. Einarsdottir, CO impedes superfast O_2 binding in ba_3 cytochrome oxidase from *Thermus thermophilus*, Proc. Natl. Acad. Sci. U. S. A. 107 (2010) 21010–21015.
[32] V. Rauhamäki, M. Wikström, The causes of reduced proton-pumping efficiency in type B and C respiratory heme-copper oxidases, and some mutated variants of type A, Biochim. Biophys. Acta 1837 (2014) 999–1003.
[33] H. Han, J. Hemp, L.A. Pace, H. Ouyang, K. Ganesan, J. Hyeob Roh, F. Daldal, S.R. Blanke, R.B. Gennis, Adaption of aerobic respiration to low O_2 environments, Proc. Natl. Acad. Sci. U. S. A. 108 (2011) 14109–14114.
[34] V. Rauhamäki, D.A. Bloch, M. Wikström, Mechanistic stoichiometry of proton translocation by cytochrome cbb_3, Proc. Natl. Acad. Sci. U. S. A. 109 (2012) 7286–7291.
[35] A.D. Becke, Density-functional thermochemistry. III. The role of exact exchange, J. Chem. Phys. 98 (1993) 5648–5652.
[36] S. Grimme, J. Anthony, S. Ehrlich, H. Krieg, A consistent and accurate *ab initio* parametrization of density functional dispersion correction (DFT-D) for the 94 elements H-Pu, J. Chem. Phys. 132 (2010) 154104.
[37] Jaguar 7.6, Schrödinger, LLC, New York, NY, 2009.
[38] M.R.A. Blomberg, P.E.M. Siegbahn, G.T. Babcock, Modeling electron transfer in biochemistry: a quantum chemical study of charge separation in *Rhodobacter sphaeroides* and photosystem II, J. Am. Chem. Soc. 120 (1998) 8812–8824.
[39] Gaussian 09, Revision C.01, Gaussian Inc., Wallingford, CT, 2010.
[40] M.R.A. Blomberg, P.E.M. Siegbahn, Mechanism for N_2O generation in bacterial nitric oxide reductase: a quantum chemical study, Biochemistry 51 (2012) 5173–5186.